

A negative ion TPC with GridPix readout

2 C. Ligtenberg^{a,*}, M. van Beuzekom^a, Y. Bilevych^b, K. Desch^b,
H. van der Graaf^a, M. Gruber^b, F. Hartjes^a, K. Heijhoff^{a,b}, J. Kaminski^b,
4 P.M. Kluit^a, N. van der Kolk^a, G. Raven^a, T. Schiffer^b, J. Timmermans^a

^a*Nikhef, Science Park 105, 1098 XG Amsterdam, The Netherlands*

6 ^b*Physikalisches Institut, University of Bonn, Nussallee 12, 53115 Bonn,
Germany*

8 Abstract

The performance of GridPix technology as a negative ion TPC readout was
10 studied using a quad module with four Timepix3 based GridPix chips. The
TPC is operated using a 93.6/5/1.4 gas mixture of Ar/iC₄H₁₀/CS₂ with a
12 small amount of oxygen and water vapor at a pressure of 1030 mbar and a
temperature of 297 K. Tracks were produced by a pulsed N₂ laser. The GridPix
14 chips are sensitive to single drift ions, and allow for the determination of the
drift distance using the minority carrier(s). The 1.56 ns time resolution of the
16 Timepix3 chips allows for a precise determination of the drift properties in the
longitudinal direction. The measured mobility of majority ion charge carriers is
18 $(1.391 \pm 0.003) \text{ cm}^2/\text{V/s}$. Using the high granularity pixel readout, the trans-
verse and longitudinal diffusion coefficients were measured to correspond to an
20 effective thermal diffusion temperature of 383 K and 305 K respectively.

Keywords: Micromegas, gaseous pixel detector, micro-pattern gaseous
22 detector, Timepix, GridPix, negative ion time projection chamber

1. Introduction

24 In a negative ion Time Projection Chamber (TPC), ionisation charge is
transported to the readout plane by negatively charged ions instead of elec-
26 trons, thereby reducing the diffusion down to the thermal limit [1]. The TPC
detects interactions that create ionisation electrons in the gas of the TPC. The
28 primary ionisation electrons are captured by the highly electronegative CS₂ gas
component, and the formed ions drift to the anode by a drift field. In the high
30 field amplification region near the anode, the electrons detach and an avalanche
occurs which is detected by the readout electronics.

32 The negative ion TPC was applied to directional dark matter searches, e.g.
in the Drift IId experiment [2]. The TPC was operated using a low pressure
34 30:10 Torr CF₄:CS₂ gas mixture. If oxygen is present in the gas mixture, extra
species of ions called minority carriers with a larger mobility are created [3].
36 From the difference in arrival time, the absolute position in the drift direction

*Corresponding author. Telephone: +31 20 592 2000
Preprint submitted to Elsevier
Email address: cligtenb@nikhef.nl (C. Ligtenberg)

can be reconstructed without the need of knowing the event time in the detector
38 [4].

In this paper an exploratory study of GridPix technology as a negative ion
40 TPC readout is presented. A GridPix consists of a CMOS pixel chip with
integrated amplification grid added by MEMS postprocessing techniques [5,
42 6]. The GridPix TPC readout has a fine granularity of $55\ \mu\text{m} \times 55\ \mu\text{m}$ and is
sensitive to single charge carriers. A negative ion TPC with GridPix readout
44 can provide an excellent spatial resolution without a magnetic field. Recently
a quad module with four Timepix3 based GridPix chips was developed in the
46 context of a future collider experiment [7]. The high single ion resolution of
the quad detector allows an accurate measurement of the resolution and an
48 experimental test of the expected low diffusion coefficient for ions. This first
investigation focuses on operation of the quad module in an already existing
50 setup at atmospheric pressure.

2. Quad detector

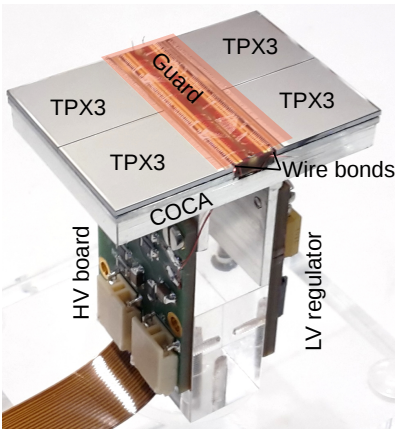


Figure 1: Picture of the quad module with four Timepix3 GridPixes (TPX3) mounted on a cold carrier plate (COCA). The central guard was omitted to show the wire bond PCB, and its operating position is indicated with a transparent rectangle. On the right the Low Voltage (LV) regulator is partially hidden behind the stump, and on the left the High Voltage (HV) board and the flexible Kapton cable are visible. This picture was previously published in [7].

52 2.1. Gridpix

The GridPix is based on the Timepix3 chip [8], which has 256×256 pixels
54 with a pitch of $55\ \mu\text{m} \times 55\ \mu\text{m}$. On the surface of the chip a $4\ \mu\text{m}$ thick silicon-
rich silicon nitride protection layer is deposited in order to prevent damage to
56 the readout electronics from discharges of the grid. On top of that, $50\ \mu\text{m}$ high

SU8 pillars support a $1\ \mu\text{m}$ thick aluminium grid with $35\ \mu\text{m}$ diameter circular
 58 holes aligned to the pixels. The Timepix3 chip has a low equivalent noise charge
 ($\approx 70\ e^-$) and can measure a precise Time of Arrival (ToA) using a 640 MHz
 60 TDC. The Timepix3 chip has a data driven readout, and is connected to a
 speedy pixel detector readout (SPIDR) board at a speed of 160 Mbps [9].

62 2.2. Quad module

The quad shown in Figure 1, consists of four GridPix chips and is optimised
 64 for a high fraction of sensitive area of 68.9%. The external dimensions are
 $39.6\ \text{mm} \times 28.38\ \text{mm}$ and it can be tiled to cover arbitrarily large areas. The
 66 four chips which are mounted on a cooled base plate (COCA), are connected
 with wire bonds to a common central 6 mm wide PCB. A 10 mm wide guard
 68 electrode is placed over the wire bonds 1.1 mm above the grids, in order to
 prevent distortion of the electric field. On the other side, the PCB is connected
 70 to a low voltage regulator. The grids are connected by $80\ \mu\text{m}$ insulated copper
 wires to a high voltage (HV) filtering board. The module consumes about 8 W
 72 of power of which 2 W in the LV regulator.

2.3. Experimental setup

74 The quad module is embedded in a box with 7 other quad modules, resulting
 in a total of 32 chips. At the moment of writing, a single quad module with
 76 4 chips can be read out per SPIDR board. Hardware to simultaneously read
 out multiple quad modules with one SPIDR board is under development. A
 78 schematic drawing of the setup is shown in Figure 2. The internal dimensions
 of the box are $79\ \text{mm} \times 192\ \text{mm} \times 53\ \text{mm}$, and it has a maximum drift length
 80 (distance between cathode and readout anode) of 40 mm. The drift field is
 shaped by a series of parallel conducting field wires of $50\ \mu\text{m}$ diameter and
 82 guard strips are located on all of the four sides of the active area. In addition,
 six guard wires are suspended above the direct boundaries of the chips. The

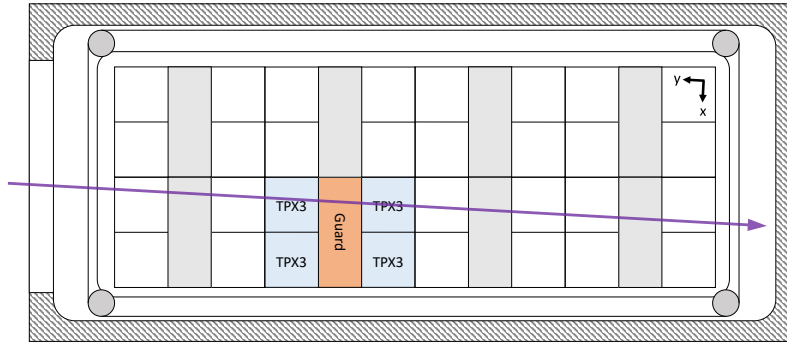


Figure 2: Schematic drawing of the 8-quad module detector with one quad in operation. In blue the laser track direction is indicated.

84 box has one Kapton window and three optical glass windows (type H-K9L) to
facilitate laser measurements.

86 The gas volume of 780 ml is continuously flushed with a 93.6/5/1.4 gas
mixture of Ar/iC₄H₁₀/CS₂ at atmospheric pressure. The gas is argon based
88 because of the dual use of the setup for detector development for future colliders,
the isobutane gas was added as a quencher to absorb UV photons produced in
90 the avalanches, and the CS₂ concentration is chosen high enough to capture
electrons shortly after the ionisation ($\lesssim 200 \mu\text{m}$). A small amount of oxygen
92 (650 ppm–1150 ppm) and water vapor (about 4000 ppm) are present in the drift
volume because of diffusion and outgassing of some of the materials. A few ppb
94 of tetra-methyl-phenylene-diamine (TMPD) molecules are added to enhance
laser ionisation in the gas. During data taking, the temperature was 297 K and
96 the pressure was 1030 mbar. The experimental parameters are summarised in
Table 1.

98 The grid voltage is set to -380 V providing an amplification field strength
of 76 kV/cm . A hit is registered if the charge on a pixel pad is above the
100 threshold set to 55 DAC counts or about $515 e^-$. The mean time over threshold
of the selected hits is $0.45 \mu\text{s}$. From this, the gain can be determined to be
102 approximately 1500 and the detection efficiency is expected to be 66%. A higher
gain and detection efficiency might be achieved by further lowering the grid
104 voltage.

Tracks of ionisation are created by a pulsed 337 nm N₂ laser at a rate of 2.5 Hz
106 with a pulse duration of 1 ns [10]. The laser is operated using the MOPA (Master
Oscillator Power Amplifier) principle to obtain a beam near the diffraction limit.
108 The parallel beam can accurately be directed in the gas volume by means of
two remotely controlled stages.

110 Data was taken in a series of nine automated experimental runs. During a
run, the drift field was set to a specific strength. The beam was positioned at
112 six different drift distances 6 mm apart. Measurements of 2400 laser shots per
run are taken in a time frame of approximately 17 minutes.

Table 1: Overview of the experimental parameters. The ranges indicate the variation over the total data taking time

Number of runs	9
Run duration	17 minutes
E_{drift}	100 – 500 V/cm
V_{grid}	-380 V
Threshold	$515 e^-$
Temperature	295.9 – 297.0 K
Pressure	1030 – 1029 mbar
Oxygen concentration	650 – 1150 ppm
Water vapor concentration	$\sim 4000 \text{ ppm}$

114 **3. Analysis**

116 In the analysis the laser position is compared to the reconstructed position
 118 from the quad detector. To reduce noise, only hits with a time over threshold
 120 above $0.1 \mu\text{s}$ are considered. The recorded stage position is taken as the reference
 122 to which the four chips are aligned by rotation in two dimensions, and shifts in
 124 the two dimensions perpendicular to the laser beam. The position of detected
 126 ionisation in the pixel plane is a direct translation from the pixels column (x -
 direction) and row number (y -direction). From the known laser pulse time, the
 z -position can be calculated as the product of the measured drift time t and
 the drift velocity v_{drift} . To clean up further the data set, hits are required to
 be within 2 mm of a laser track in the x -direction and to be within 5 mm of the
 laser track in the z -direction. The alignment and the measurement of the drift
 velocity is an iterative process.

128 An example of a resulting drift time spectrum is shown in Figure 3 for
 the run at a drift field strength E_{drift} of 300 V/cm. Other experiments using
 low pressure gas mixtures containing CS_2 and oxygen could distinguish three
 130 different minority carriers as separate peaks in the drift time spectrum [3]. In
 contrast, in our measurements only one secondary peak can be found, which is
 132 slightly broader than the first one. This could be due to e.g. overlapping drift
 time distributions, the much lower oxygen concentration, or the much higher
 134 water vapor concentration in our gas mixture affecting the minority carrier(s)
 production.

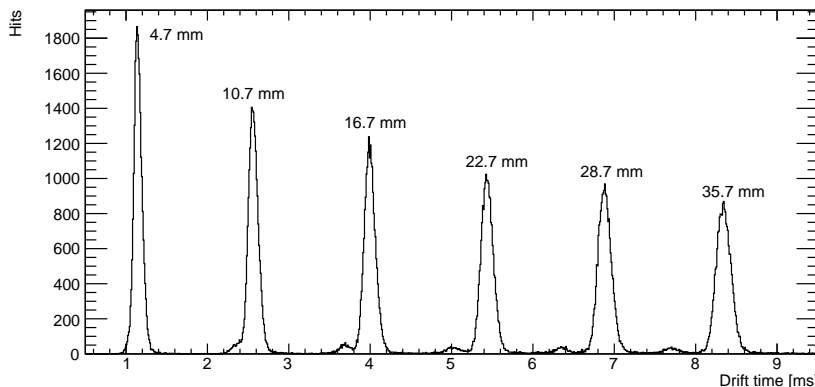


Figure 3: Drift time distribution for 400 laser pulses per z -position, annotated with the drift distance as recorded by the laser stage.

136 In order to determine the drift properties, a ‘global’ fit is made per run with
 measurements at different drift distances for a given electric field strength. The
 138 drift time t is fitted with a combination of two Gaussian distributions per laser

z-position:

$$\begin{aligned} & \frac{(1 - f_2 - f_{\text{noise}})n_{\text{hits}}}{\sigma_1\sqrt{2\pi}} \exp\left(-\frac{(t - \mu_1)^2}{2\sigma_1^2}\right) \\ & + \frac{f_2 n_{\text{hits}}}{\sigma_2\sqrt{2\pi}} \exp\left(-\frac{(t - r_2\mu_1)^2}{2\sigma_2^2}\right) + f_{\text{noise}}n_{\text{hits}}, \end{aligned} \quad (1)$$

140 where n_{hits} is the number of hits. Four parameters are different for each drift
 142 distance, and two parameters are the same for all drift distances. The mean
 time μ_1 , the standard deviation of the majority carrier distribution σ_1 , the
 standard deviation of the minority carrier(s) distribution σ_2 and a parameter
 144 f_{noise} representing a flat noise distribution, are fitted per drift distance. In the
 fit, the fraction of the number ions from minority carrier(s) f_2 and the ratio of
 146 majority carrier mobility to the minority carrier(s) mobility r_2 are equal for all
 drift distances.

148 4. Performance

4.1. Number of hits

150 The total number of detected hits is shown in Figure 4. The number of hits
 can be tuned by adjusting the laser intensity. In this gas, a minimum ionising
 152 particle is expected to create about 100 ionisation pairs per cm, of which about
 70 will be detected as hits per cm. An example event display for ionisation for
 154 a single laser pulse is shown in Figure 5.

4.2. Drift velocity measurements

156 The average drift times for the majority and minority charge carrier(s) are
 plotted as a function of the drift distance in Figure 6 for a drift field strength of
 158 300 V/cm. The drift velocity of the minority carrier is found to be 8.1% higher
 than that of the majority carrier.

160 The drift velocity of the majority carrier v_{drift} as function of the electric field
 is shown in Figure 7. The mean measured mobility is (1.391 ± 0.003) cm²/V/s.
 162 The uncertainty of the measured mobility is estimated as the r.m.s. of the given
 values, and is probably dominated by fluctuations in the (local) temperature
 164 and gas composition. Because of the unique gas composition the mobility can-
 not directly be compared to the results from other experiments. However, the
 166 mobility is the same order of magnitude as previous measurements using gas
 mixtures containing CS₂ and argon [1], and mixtures containing CS₂ and helium
 168 [11].

4.3. Diffusion measurements

170 As the ions drift towards the readout plane, they diffuse which gives them
 a Gaussian spread in the longitudinal and transverse direction. The amount of
 172 diffusion is characterised by the standard deviation of the Gaussian distribution
 σ_i , where i the longitudinal direction z or the transverse direction x . This can
 174 be expressed as

$$\sigma_i^2 = \sigma_{i0}^2 + D_i^2 z, \quad (2)$$

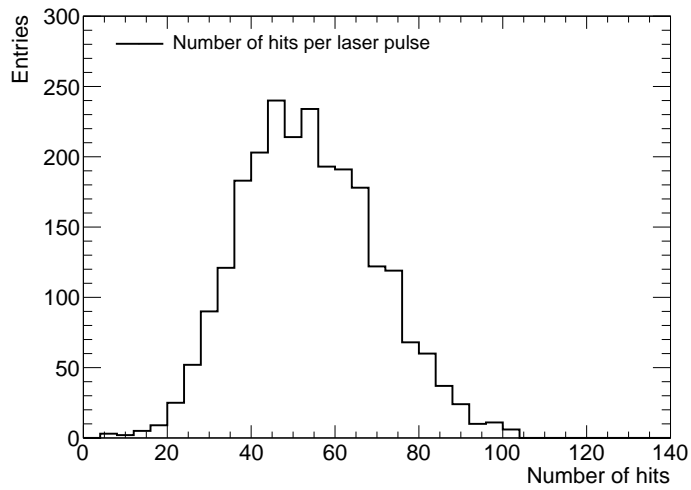


Figure 4: Total number of hits per laser track for all chips

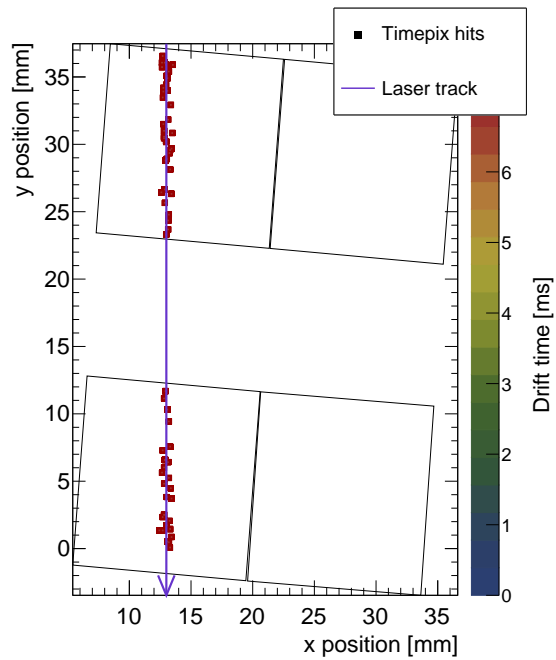


Figure 5: Example of the detected ionisation from one laser pulse with 64 hits in total. The position of the laser track (blue line) and chip edges (black outlines) are drawn in global coordinates. The pixel hits are not to scale.

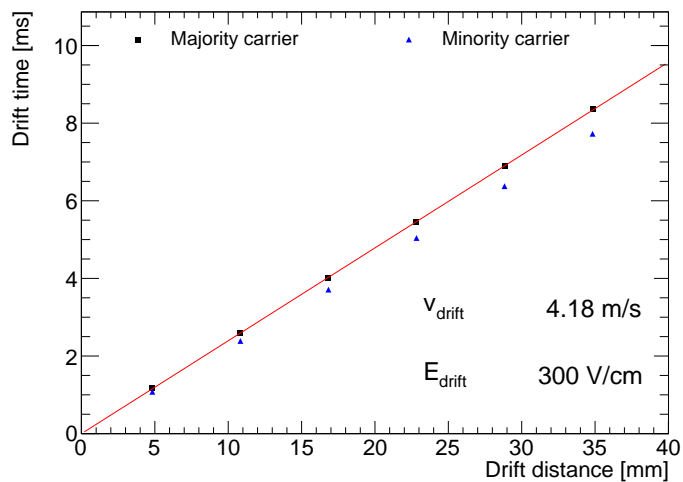


Figure 6: Drift time as a function of z -position for the majority and minority carriers

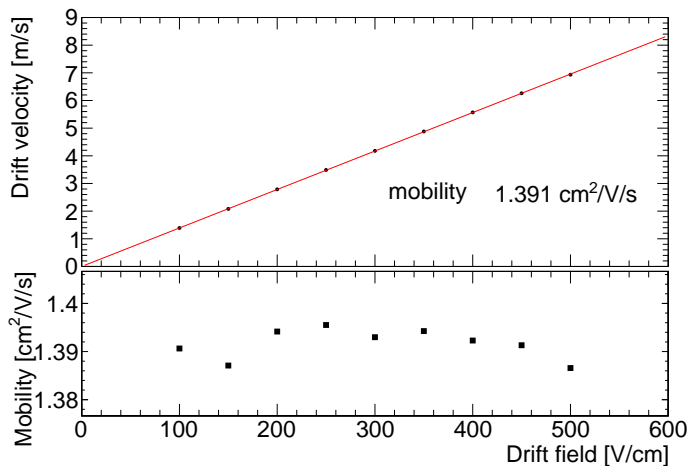


Figure 7: Drift velocity of the majority carrier ion as a function of the drift field. The mobility is acquired from a straight line fit constrained to pass through the origin (0,0).

where σ_{i0} is the standard deviation at zero drift, D_i the diffusion coefficient, and z the drift distance.

The standard deviation is acquired from a fit to the data of one Gaussian in the transverse direction, or the sum of two Gaussian functions in the longitudinal direction, see Equation (1). The drift time is converted to a distance using the measured drift velocity v_{drift} . As an example, the standard deviation as a function of drift distance for the run at a drift field strength E_{drift} of 300 V/cm is shown in Figure 8.

The constant contribution in Equation 2 is roughly independent of the electric field, and found to be $\sigma_{x0} = (94 \pm 3) \mu\text{m}$ in the transverse direction which can predominantly be attributed to the laser beam width plus some small per shot variation. In the longitudinal direction $\sigma_{z0} = (141 \pm 8) \mu\text{m}$ is measured. This can predominantly be attributed to the laser beam width plus per shot variations, or unrecognised minority carrier(s).

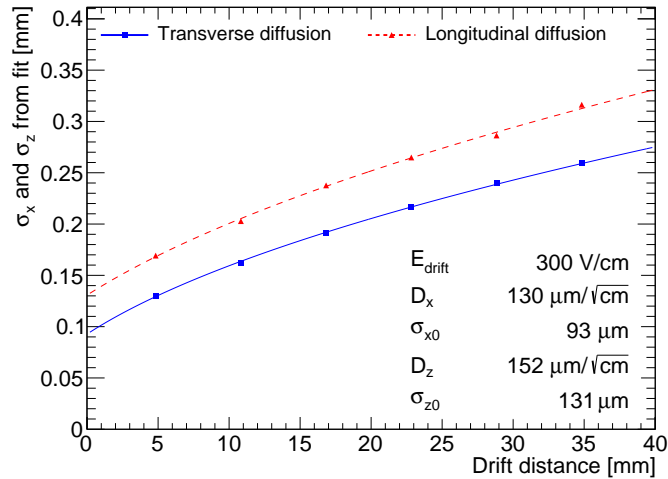


Figure 8: Standard deviation of hit positions in the transverse and longitudinal direction as a function of drift distance. The data is fitted with Equation (2).

The diffusion coefficient depends on the electric field strength, and the measurements are shown in Figure 9. At low drift field strengths, the ions have thermal energy and the diffusion coefficient can be expressed as

$$D_{\text{thermal}} = \sqrt{\frac{2k_{\text{B}}T}{eE}}, \quad (3)$$

where k_{B} is the Boltzmann constant, T is the temperature of the gas, e is the charge of the ion, and E is the electric field strength (see e.g. [12]). Both the transverse and longitudinal diffusion coefficients are fitted with Equation (3) with the temperature T as a free parameter. The transverse diffusion corre-

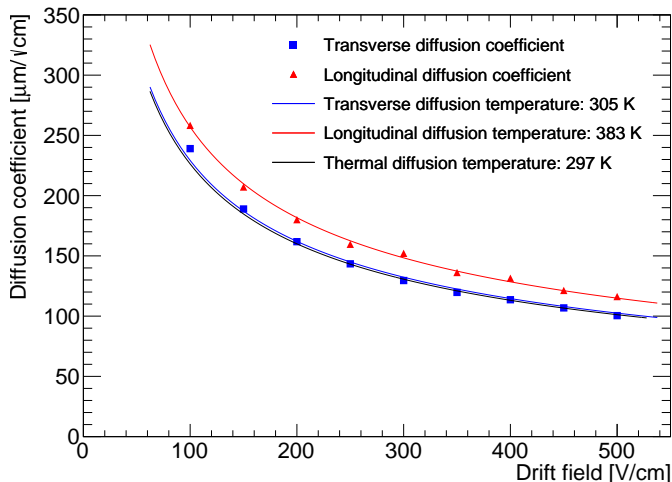


Figure 9: Diffusion coefficients in the longitudinal and transverse directions as a function of the drift field E . Both are fitted with Equation (3). For comparison the expectation for thermal diffusion is shown.

196 sponds to an effective temperature of 305 K, which is close to the gas temper-
 197 ature. The effective temperature of the longitudinal diffusion is rather high,
 198 383 K. This could be explained by the spread on the distance that electrons
 199 travel before they are captured by the CS_2 molecules, or unrecognised minority
 200 carrier(s). Another explanation is the possible spontaneous detachment of the
 201 electron and the CS_2 molecule, allowing the electron to drift for a short distance
 202 before being captured again by another CS_2 molecule. A simple thermal model
 203 with a $1/\sqrt{E_{\text{drift}}}$ dependence describes the data well. In both cases, the main
 204 source of uncertainty is (local) temperature fluctuations and variations in the
 gas composition.

205 In other experiments using a low pressure CS_2 gas, the longitudinal diffusion
 206 is found to be in agreement with the thermal values [13]. In a 500 Torr He and
 207 200 Torr CS_2 gas mixture, longitudinal diffusion coefficients slightly below to
 208 the thermal values are found [11].

210 4.4. Reconstruction of drift distance

211 The difference in drift velocity between the majority carrier and minority
 212 carrier(s) can be used to reconstruct the absolute position in the drift direction.
 213 Previously, this technique was demonstrated in a 30:10:1 Torr $\text{CF}_4:\text{CS}_2:\text{O}_2$ gas
 214 mixture with a spread on the reconstructed drift distance of ± 2 cm [4]. A
 215 precision of 16 mm was achieved using a similar technique using an SF_6 gas [14].

216 Here, fiducialisation is applied to data from the run at the largest drift
 217 field of 500 V/cm which gives the best signal peak separation, and also has the
 218 highest oxygen concentration of about 1150 ppm. About 4.4% of the hits are

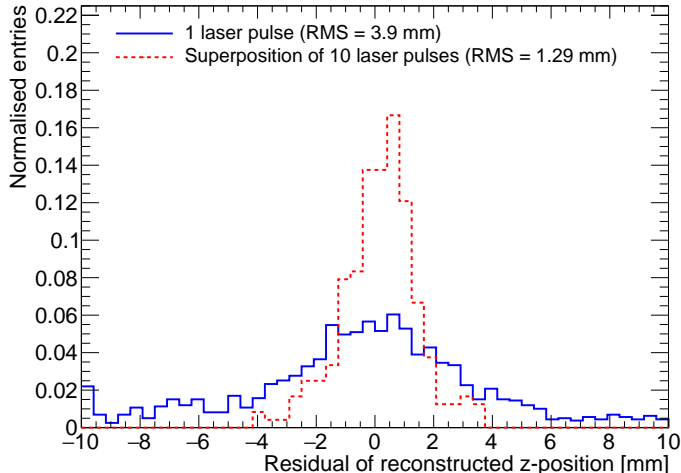


Figure 10: Residual of reconstructed z -position for 2401 laser pulses with a mean number of 43 detected ions and for 240 superpositions of ten laser pulses with a total mean number of 429 ions. The r.m.s. of the reconstructed z -positions for the single laser pulse is calculated for the 66% of the entries that fall inside the axis range.

220 attributed to the minority carrier(s), whose mobility is 8.1% higher than that of the majority carrier.

222 The reconstruction proceeds by performing per event a maximum likelihood fit of Equation (1) to the measured relative arrival time of ions from one or more laser pulses. A new parameter t_0 is introduced to absorb the now unknown laser pulse time. The parameters f_2 , r_2 , f_{noise} are fixed to their previously fitted values. For σ_1 Equation (2) is used, and σ_2 is by approximation fixed to σ_1 . The parameter μ_1 (the mean arrival time of the primary carrier peak) are acquired from the fit. The z -position is calculated using the measured drift velocity v_{drift} . The detected spread in the transverse direction is not utilised in the determination of the z -position.

230 By comparing the reconstructed z -position to the z -position of the laser stage for all six drift distances, the residual shown in Figure 10 is obtained. From a single laser pulse, on average 43 ions are detected and the r.m.s. of the distribution is 3.9 mm for the 64% of the laser pulses that fall within the ± 10 mm range. The determined z -position has a rather large spread, because very few minority carrier(s) ions are detected. In order to estimate the performance for a larger number of ions, a superposition of ten laser pulses at the same z -position is made by shifting their arrival times by the time difference between the laser pulses. From this we acquire emulated pulses with a mean number of 429 detected ions, which the quad is still able to detect without occupancy problems. The resulting r.m.s. is 1.29 mm for the combined laser pulses and all 240 of the entries are within the ± 10 mm range.

242 5. Conclusions and outlook

The performance of GridPix technology as a negative ion TPC readout was
244 studied using a quad module with four Timepix3 based GridPix chips. The
TPC is operated using a 93.6/5/1.4 gas mixture of Ar/iC₄H₁₀/CS₂ with a small
246 amount of oxygen and water vapor at a pressure of 1030 mbar and a temperature
of 297 K. Tracks were produced by a pulsed N₂ laser. The 1.56 ns time resolution
248 of the Timepix3 chips allows for a precise determination of the drift properties in
the longitudinal direction. The measured mobility is $(1.391 \pm 0.003) \text{ cm}^2/\text{V/s}$.
250 Using the high granularity pixel readout, the transverse and longitudinal diffusion
coefficients were measured to correspond to an effective thermal diffusion
252 temperature of 383 K and 305 K. A simple thermal model with a $1/\sqrt{E_{\text{drift}}}$
dependence describes the data well. This confirms the expected low diffusion
254 coefficient for ions. Furthermore, the GridPix has an efficiency of approximately
66% to detect single drift ions. By using the minority carriers, the z -position
256 can be measured with an expected precision of 1.29 mm using 429 ions.

In the future, a GridPix TPC readout might be of interest to directional
258 dark matter experiments. The often desired operation at low pressure can be
investigated in combination with a GridPix readout. For these experiments gas
260 mixtures containing SF₆ have some advantages [13], and can also be studied for
operation with a GridPix readout. Alternatively, for operation around atm-
262 spheric pressure replacing Argon with the lighter Helium could increase nuclear
recoils lengths important for directional dark matter searches [15].

264 All in all, the fine granularity and high timing precision of the GridPix TPC
readout in combination with a good single ion detection efficiency, provide an
266 excellent position resolution in the longitudinal and transverse direction.

Acknowledgements

268 This research was funded by the Netherlands Organisation for Scientific Re-
search NWO. The authors want to acknowledge the support of the mechanical
270 and electronics departments at Nikhef.

References

- 272 [1] C. Martoff, D. Snowden-Ifft, T. Ohnuki, N. Spooner, M. Lehner, Suppress-
ing drift chamber diffusion without magnetic field, Nucl. Instrum. Meth. A
274 440 (2000) 355–359. doi:10.1016/S0168-9002(99)00955-9.
- [2] J. Battat, et al., Low Threshold Results and Limits from the DRIFT
276 Directional Dark Matter Detector, Astropart. Phys. 91 (2017) 65–74.
arXiv:1701.00171, doi:10.1016/j.astropartphys.2017.03.007.
- 278 [3] D. P. Snowden-Ifft, Discovery of Multiple, Ionization-Created Anions in
Gas Mixtures Containing CS₂ and O₂ (8 2013). arXiv:1308.0354.

- 280 [4] J. Battat, et al., First background-free limit from a directional dark matter
282 experiment: results from a fully fiducialised DRIFT detector, *Phys. Dark
Univ.* 9-10 (2015) 1–7. [arXiv:1410.7821](https://arxiv.org/abs/1410.7821), [doi:10.1016/j.dark.2015.06.001](https://doi.org/10.1016/j.dark.2015.06.001).
- 284 [5] P. Colas, A. P. Colijn, A. Fornaini, Y. Giomataris, H. van der Graaf,
286 E. H. M. Heijne, X. Llopart, J. Schmitz, J. Timmermans, J. L. Visschers,
The readout of a GEM- or micromegas-equipped TPC by means of the
288 Medipix2 CMOS sensor as direct anode, *Nucl. Instrum. Meth. A* 535 (2004)
506–510. [doi:10.1016/j.nima.2004.07.180](https://doi.org/10.1016/j.nima.2004.07.180).
- [6] M. Campbell, M. Chefdeville, P. Colas, A. P. Colijn, A. Fornaini,
290 I. Giomataris, H. van der Graaf, E. H. M. Heijne, P. Kluit, X. Llopart-
Cudie, J. Schmitz, J. Timmermans, J. L. Visschers, Detection of single elec-
292 trons by means of a micromegas-covered MediPix2 pixel CMOS readout cir-
cuit, *Nucl. Instrum. Meth. A* 540 (2005) 295–304. [arXiv:physics/0409048](https://arxiv.org/abs/physics/0409048),
294 [doi:10.1016/j.nima.2004.11.036](https://doi.org/10.1016/j.nima.2004.11.036).
- [7] C. Ligtenberg, et al., Performance of the GridPix detector quad, *Nucl.*
296 *Instrum. Meth. A* 956 (2020) 163331. [arXiv:2001.01540](https://arxiv.org/abs/2001.01540), [doi:10.1016/
j.nima.2019.163331](https://doi.org/10.1016/j.nima.2019.163331).
- 298 [8] T. Poikela, J. Plosila, T. Westerlund, M. Campbell, M. De Gaspari,
X. Llopart, V. Gromov, R. Kluit, M. van Beuzekom, F. Zappone,
300 V. Zivkovic, C. Brezina, K. Desch, Y. Fu, A. Kruth, Timepix3: a 65K
channel hybrid pixel readout chip with simultaneous ToA/ToT and sparse
302 readout, *Journal of Instrumentation* 9 (05) (2014) C05013.
URL <http://stacks.iop.org/1748-0221/9/i=05/a=C05013>
- 304 [9] B. van der Heijden, J. Visser, M. van Beuzekom, H. Boterenbrood, S. Kulis,
B. Munneke, F. Schreuder, SPIDR, a general-purpose readout system for
306 pixel ASICs, *JINST* 12 (02) (2017) C02040. [doi:10.1088/1748-0221/12/
02/C02040](https://doi.org/10.1088/1748-0221/12/02/C02040).
- 308 [10] F. Hartjes, A diffraction limited nitrogen laser for detector calibration in
high energy physics, Ph.D. thesis, University of Amsterdam (1990).
- 310 [11] C. Martoff, R. Ayad, M. Katz-Hyman, G. Bonvicini, A. Schreiner, Negative
ion drift and diffusion in a TPC near 1 bar, *Nucl. Instrum. Meth. A* 555
312 (2005) 55–58. [arXiv:physics/0406114](https://arxiv.org/abs/physics/0406114), [doi:10.1016/j.nima.2005.08.
103](https://doi.org/10.1016/j.nima.2005.08.103).
- 314 [12] W. Blum, L. Rolandi, W. Riegler, Particle detection with drift cham-
bers, *Particle Acceleration and Detection*, Springer, 2008. [doi:10.1007/
978-3-540-76684-1](https://doi.org/10.1007/978-3-540-76684-1).
316 URL <https://www.springer.com/gp/book/9783540766834>
- 318 [13] N. Phan, R. Lafler, R. Lauer, E. Lee, D. Loomba, J. Matthews, E. Miller,
The novel properties of SF₆ for directional dark matter experiments, *JINST*

- 320 12 (02) (2017) P02012. [arXiv:1609.05249](#), [doi:10.1088/1748-0221/12/02/P02012](#).
- 322 [14] T. Ikeda, T. Shimada, H. Ishiura, K. Nakamura, T. Nakamura, K. Miuchi,
324 Development of a Negative Ion Micro TPC Detector with SF₆ Gas for the
Directional Dark Matter Search (4 2020). [arXiv:2004.09706](#).
- [15] E. Baracchini, G. Cavoto, G. Mazzitelli, F. Murtas, F. Renga, S. Tomassini,
326 Negative Ion Time Projection Chamber operation with SF₆ at nearly at-
328 mospheric pressure, JINST 13 (04) (2018) P04022. [arXiv:1710.01994](#),
[doi:10.1088/1748-0221/13/04/P04022](#).